**REVIEW**　　　　　　　　　　　　　　　　　　　　　　　　　　　　**Open Access**

Check for
updates

# Photoacoustic imaging of cells in a three-dimensional microenvironment

Wei-Wen Liu[1] and Pai-Chi Li[1,2*] ⓘD

## Abstract

Imaging live cells in a three-dimensional (3D) culture system yields more accurate information and spatial visualization of the interplay of cells and the surrounding matrix components compared to using a two-dimensional (2D) cell culture system. However, the thickness of 3D cultures results in a high degree of scattering that makes it difficult for the light to penetrate deeply to allow clear optical imaging. Photoacoustic (PA) imaging is a powerful imaging modality that relies on a PA effect generated when light is absorbed by exogenous contrast agents or endogenous molecules in a medium. It combines a high optical contrast with a high acoustic spatiotemporal resolution, allowing the noninvasive visualization of 3D cellular scaffolds at considerable depths with a high resolution and no image distortion. Moreover, advances in targeted contrast agents have also made PA imaging capable of molecular and cellular characterization for use in preclinical personalized diagnostics or PA imaging-guided therapeutics. Here we review the applications and challenges of PA imaging in a 3D cellular microenvironment. Potential future developments of PA imaging in preclinical applications are also discussed.

**Keywords:** Photoacoustic imaging, Biomedical imaging, Three-dimensional cell culture, Tumor microenvironment

## Introduction

In the past few decades, the conventional 2D cell cultures have remarkably increased the knowledge in basic cell biology and preclinical biomedical applications. However, cells cultured in a 2D monolayer lack a typical 3D architecture. Moreover, cells inhabiting a rigid surface without a 3D elastic fibrous meshwork (i.e., the extracellular matrix [ECM]) cannot normally response the physical or biochemical cues from the surrounding physiological matrix substrate [1–5]. Recently, in efforts to target the tumor microenvironment for improving both the effectiveness and efficiency of cancer therapeutics, several studies such as immunotherapy, tumor vasculature, or ECM remodeling has been led to a new era and yielded novel insights [6–8]. For example, extravasated T lymphocytes infiltrated into the stromal ECM for migrating to the targeted tumor sites has been demonstrated in 3D cell culture models [9–11]. An amoeboid shape change and contact guidance during T-cell locomotion in 3D collagen fibrils has been documented as a protease-independent process, but it should be dependent on protease in a dense collagen fibrillar meshwork with size-limiting pores [9, 10, 12–15]. A similar model for tumor cell migration in the stromal ECM has also been described [13, 15]. Tumor cell intravasation and extravasation through the vascular wall to other organs is a critical step of tumor migration and metastasis [16]. 3D cell cultures have been utilized in biomimetic models of the tumor vasculature or angiogenesis for investigating the intrinsic or extrinsic modulation of the tumor vascular niche [17–20]. Preclinical studies of the normalization of tumor vasculature or drug screening for anti-angiogenesis have also been performed [21, 22]. 3D culture models can recapitulate partial physiological diversity and thereby allow for dissecting underlying regulatory mechanisms into separate units within a controllable microenvironment. The examinations performed in these studies may help to improve therapeutic interventions and inform clinical decisions.

The availability of appropriate imaging modalities for analyzing cell dynamics within 3D cell culture systems can facilitate interpretations and precise quantification. High-resolution imaging systems such as laser-scanning confocal microscopy, electron microscopy, and multi-photon microscopy are usually employed by researchers to quantify and track cell behaviors. However, 3D cell

* Correspondence: paichi@ntu.edu.tw
[1]Graduate Institute of Biomedical Electronics and Bioinformatics, National Taiwan University, Taipei, Taiwan
[2]Department of Electrical Engineering, National Taiwan University, Taipei, Taiwan

cultures are usually thick and exhibit strong light scattering, which results in the impinging light experiencing severe diffraction and diffusion. One method for acquiring images of high quality during live cell imaging is to culture cells on the surface of a thin layer of 3D ECM matrix gel (also named a 2.5D culture) or a cell-laden 3D ECM matrix gel with a reduced thickness. Microscope objective lenses with numerical apertures (NA) necessary for high-resolution imaging have very small working distances, such as 100–200 μm for lenses with magnifications above 60×. When using an inverted microscope, the thickness of the holder (e.g., coverslip or polydimethylsiloxane layer) supporting the 3D cell culture will reduce the working distance to 0–50 μm, and so the deepest visible site of the 3D gel will be only 50 μm from the bottom surface of the holder. However, when the thickness of a hydrogel is less than 50 μm, a finite-element model simulated that the hydrogel stress field around the indenter actually interacted with the rigid bottom support, leading to a stiffer response [23]. Experimental evidence further proves that the cell aspect ratio, area, and migration speed are significantly increased in hydrogel with a height of less than 200 μm due to the mechanical gradient along its height [23]. Moreover, although yes-associated protein (YAP) has been documented as a key factor to mediate cancer progression through mechanotransduction, a recent report challenges the established knowledge that the breast cancer progression is regulated by YAP-dependent mechanotransduction in 2.5D culture model, which is, the independency of YAP in ECM stiffness-mediated breast cancer progression is found in 3D cultures and patient samples [24]. Therefore, data obtained from 2.5D cultures and thin cell-laden 3D cultures should be examined carefully. Obtaining detailed information about the center region of 3D cell cultures usually requires the biochemical processing of gel fixation following by thin sections of embedded gels to produce samples whose structural, histological, or protein expression patterns can be investigated using optical imaging systems. Regrettably, these processing methods can cause gel deformation or damage, the loss of localized enzymes and metabolite profiles, and alterations to cell dynamics and chemical and nutrient gradients.

To address the problem of deep imaging, PA imaging as a noninvasive and hybrid imaging modality that combines optical excitation and ultrasonic detection to attain better spatial resolution than traditional ultrasound (US) imaging and also achieve deeper penetration than purely optical imaging systems. PA imaging is a powerful imaging technique that can provide scalable and multicontrast images of 3D cell culture scaffolds, ranging from single cells to an organoid culture. Furthermore, both structural and functional information can be obtained using a single- or multiwavelength laser. Conventional optical imaging using contrast agents with emitted fluorescence or bioluminescence, which typically can be imaged with spatial resolution and the imaging depth in micrometer or sub-micrometer scale. By taking the advantage of the laser-based PA principles, photons can be converted into ultrasonic waves in biological samples. Because of acoustic wave can travel through scattering tissue much far than photon does, PA imaging techniques can surpass the depth limitation of optical imaging systems. To provide a practical guide for choosing the appropriate technologies to examine the 3D structural or functional information of biomaterials, cellular behaviors, and cell–biomaterial interactions, we compare the properties of the most widely used imaging modalities to that of PA imaging modality (Table 1). As such, we summarized the scalability, the chemical sensitivity, and the potential applications of acoustic imaging, optical imaging, PA imaging, and electron imaging. Among these techniques, PA imaging can achieve better spatial resolution than acoustic imaging, and its imaging depth can be larger than optical imaging and electron imaging. In this review, we first briefly outline the importance of using 3D cell cultures as novel physiological mimicry platforms, and then discuss the current challenges in optic-based imaging of 3D cell cultures for the characterization of cell–biomaterial interactions. Since PA imaging can potentially obtain images at greater depths, we describe the physical background into how PA imaging works and the principles of the two main PA imaging modalities. Combining PA imaging with the use of multiplex contrast agents makes it possible to monitor interactions between cells and 3D scaffolds. Since most 3D cell cultures have no endogenous contrast agents, the application of exogenous contrast agents in 3D cell cultures will be more focused in this review. Finally, we draw conclusions about the current bottlenecks and the future outlook on expanding the capabilities of PA imaging through the use of multimodality and unconventional imaging toolkits.

## Review
### Fundamentals of PA imaging

PA imaging is based on the physical integration of optical irradiation and ultrasonic detection (Fig. 1) [25–27]. Irradiating light-absorbing materials with a short-pulse laser induces an increase in pressure through thermoelastic expansion. The resulting pressure waves can be interpreted to US waves as the pressure wavefront propagates in the light-absorbing region. The US waves, also known as PA waves, can be detected by US transducers to produce electrical signals. These signals are then amplified, digitized, decoded, and transferred to a computer for image formation. The amplitude of the PA response is proportional to the concentration of the

**Table 1** Comparison of properties of the imaging modalities[a]

| Imaging modality | Spatial resolution | Imaging depth | Chemical sensitivity | Potential applications |
|---|---|---|---|---|
| EM | 1 nm | 0.1 μm | N.A. | Biomineralization, biomaterial surface structure, pore formation, cell–biomaterial interaction |
| CM | 0.4 μm | 0.1 mm | High | Cell behavior, cell tracking, gene expression, cellular substructure, functional activity |
| MPM | 1 μm | 1 mm | High | Biomaterial architecture, cell tracking, functional activity |
| OR-PAM | 2.5 μm | 1 mm | High | Cell tracking, functional activity, fluid dynamics, cell–biomaterial interaction |
| OCT | 10 μm | 2 mm | Low | Vascularization, biomaterial architecture, functional activity |
| AR-PAM | 45 μm | 3 mm | High | Vascularization, biomaterial architecture, cell metabolism, functional activity |
| US (20 MHz) | 165 μm | 3 cm | Low | Fluid dynamics, mechanics, spatial patterning of cells, functional activity |

[a]*Abbreviations: EM* electron microscopy, *CM* confocal microscopy, *MPM* multi-photon microscopy, *OR-PAM* optical resolution photoacoustic microscopy, *OCT* optical coherence tomography, *AR-PAM* acoustic resolution photoacoustic microscopy, *US* ultrasound imaging, *N.A.* not available

absorbers, the optical absorption coefficient of the photoabsorber, and the thermal coefficient of volume expansion. The contrast of PA imaging when imaging in vivo or in vitro samples can be improved by utilizing the various available PA contrast agents as photoabsorbers such as hemoglobin and gold nanoparticles [28–33].

## Photoacoustic microscopy

Photoacoustic microscopy (PAM) is one type of PA imaging modality that aims to image at millimeter-scale depths and micrometer-scale resolutions. Its microscopic essence is appropriate for visualizing structural, functional, or molecular information such as property alterations of a scaffold, cellular dynamics, or engineered vasculature and angiogenesis inside 3D-scaffold-based samples. During PAM scanning, each laser-pulse-generated time-resolved PA signal recorded from the US transducer is converted into one-dimensional depth-resolved image (A-line) based on the sound velocity in the sample, and A-line scanning is used to form a 2D frame. Coupling this with 2D raster scanning along the horizontal plane allows a 3D image with volumetric information to be generated. Because the degree of scattering is much lower for US than for visible light in biological samples, PAM provides a better spatial resolution and a deeper penetration depth [34, 35].

The axial resolution and the achievable penetration depth of PAM are determined by the central frequency of the US transducer. The axial resolution is equal to half the spatial pulse width, and a higher operating frequency has a smaller wavelength and hence generates shorter pulses, giving a better axial resolution. The lateral resolution of PAM is determined by the combined response of the point source from overlapping optical excitation and acoustic detection by the PAM imaging system, known as the point spread function. Depending on what directs the resolution of the imaging system, PAM can be further categorized into optical-resolution PAM (OR-PAM) and acoustic-resolution PAM (AR-PAM) (Fig. 2). In OR-PAM, the optical focus is better than the acoustic focus and a lateral resolution of a few micrometers can be achieved, allowing for single-cell imaging. Nonetheless, high optical scattering limits the
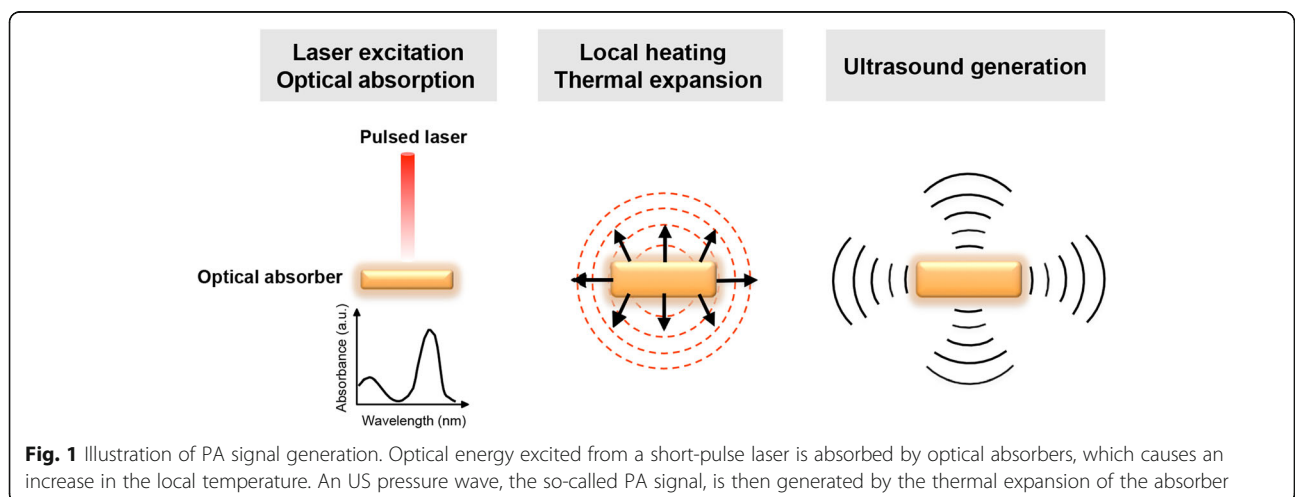


**Fig. 1** Illustration of PA signal generation. Optical energy excited from a short-pulse laser is absorbed by optical absorbers, which causes an increase in the local temperature. An US pressure wave, the so-called PA signal, is then generated by the thermal expansion of the absorber
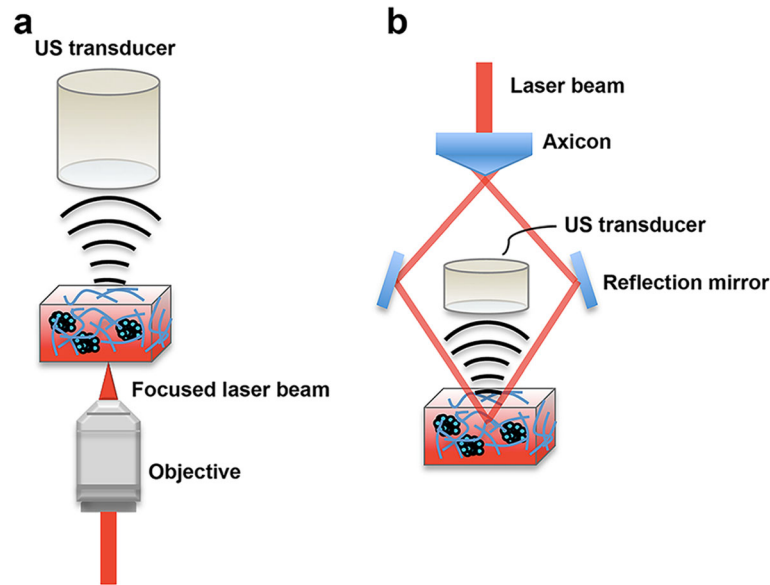
**Fig. 2** Schematics of two types of PAM system: (a) OR-PAM and (b) AR-PAM. In this setup, 3D tumor spheres labeled with contrast agents are cultured in a cuboidal matrix hydrogel for PA imaging. Note that the laser light is focused in OR-PAM but unfocused in AR-PAM, respectively. Once the laser energy is delivered into the 3D cell culture and absorbed by endogenous or exogenous contrast agents, the absorbed energy is converted into heat, leading to thermal expansion. Ultrasound signals are then generated and detected by the transducer located at the top of the samples

penetration depth to around 1 mm in OR-PAM. In AR-PAM, the acoustic focus is much better than the optical focus, and a lateral resolution of a few tens of micrometers can be achieved. The relatively weak acoustic scattering in AR-PAM allows a penetration depth of up to a few centimeters, which enables investigations of phenotypic characteristics in a 3D configuration. In both OR-PAM and AR-PAM, using objectives with low NA makes it possible to image a large field of view without sacrificing the depth resolution.

## Monitoring a 3D microenvironment using PA contrast agents and multiscale PAM

PA contrast agents can be categorized into two types, endogenous and exogenous. Two well-known endogenous contrast agents applied in in vivo label-free PA imaging are melanin and hemoglobin. Except for cells containing melanin, PA contrast is usually undetectable in biomaterials and the cell-laden 3D culture, and so an exogenous contrast agent needs to be introduced for contrast enhancement. Exogenous contrast agents for use in PA molecular imaging have to possess certain photophysical and biological properties, such as efficient optical-to-PA conversion, long-lived excited-state lifetime, biocompatibility, distinct optical absorption spectra (where the endogenous contrast agents have a lower absorption), and the capability to pass through cellular and fibrillar barriers for successful labeling [29, 36]. Furthermore, both endogenous and exogenous contrast agents

are usually with optical absorption spectra in the near-infrared (NIR) window (600–1100 nm) so as to ensure their deeper penetration and hence the required imaging depth.

For multiscale biological systems, several kinds of representative PAM systems are summarized based on the scalable imaging performance shown in Fig. 3 [44]. Generally, AR-PAM (i.e. using unfocused laser beam) can achieve imaging depth beyond 1 mm, in contrast, OR-PAM can only achieve imaging depth within 1 mm due to the limited penetration of a focused laser beam. AR-PAM with a focused 50-MHz ultrasound detector can provide lateral resolution of 45 μm and axial resolution of 15 μm for detection of oxygen saturation in a single blood vessel over 1 mm beneath the tissue surface [39]. The imaging depth can be extended to 4 cm and the lateral resolution is enlarged to 100–560 μm when reducing the center frequency of the focused ultrasound detector to 5 MHz for macroscopic purpose [38]. Real-time imaging and the deeper penetration depth up to 7 cm can be achieved when using an ultrasound transducer array as the detector combined with a computed tomography scanning system [37, 45]. OR-PAM for imaging cells has the lateral resolution of 1–5 μm, and the axial resolution can achieve to ~ 15 μm when combination with a 75-MHz focused ultrasound detector [40] and it can be improved to 7.5 μm when using focused ultrasonic detector with a center frequency of 125 MHz [41]. Combination with objectives with a higher NA and sub-diffraction techniques, the lateral resolution of OR-PAM can be increased to 87 to 220 nm to
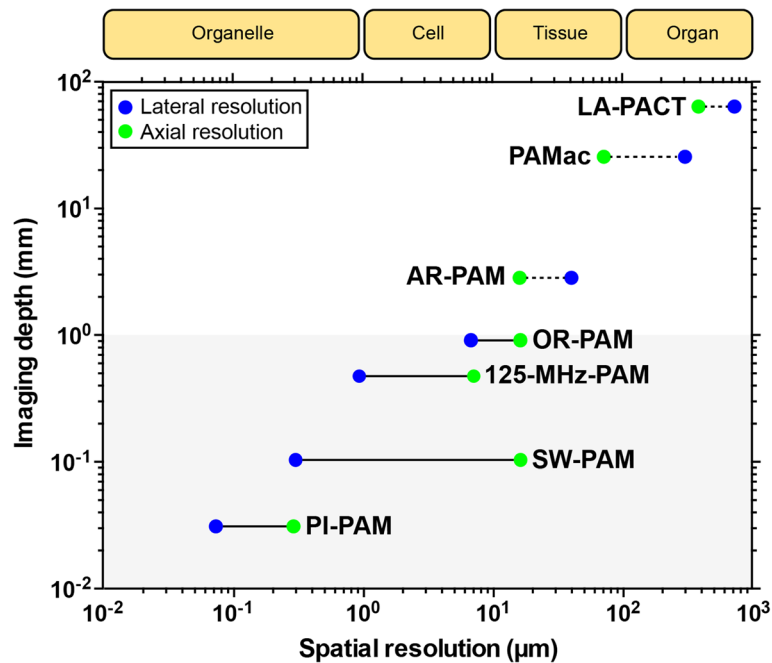
**Fig. 3** Scalability of PAM among multiscale biological systems. The blue circles denote lateral resolution, and green circles denote axial resolution. Solid lines denote OR-PAMs, and dotted lines denote AR-PAMs. LA-PACT, linear-array PA computed tomography [37]; PAMac, PA macroscopy [38]; AR-PAM, acoustic resolution PAM [39]; OR-PAM, optical resolution PAM [40]; 125-MHz-PAM, PAM using a 125-MHz ultrasound detector [41]; SW-PAM, subwavelength resolution PAM [42]; PI-PAM, photoimprint PAM [43]. Figure adapted from [44]

achieve the purpose for imaging organelle [42, 43]. Following sections will draw on the biomedical applications of PA imaging based on the properties of PA contrast agents including probing functional biological processes, structural imaging of biomaterial scaffolds and vasculature, cell tracking, and tumor detection in 3D microenvironments. Among these studies, to achieve PA imaging at the single-cell scale, OR-PAM can be used, and AR-PAM can be used to achieve deeper penetration and tissue-scale imaging in in vivo animals/human studies.

### Functional imaging of 3D cell cultures/tissues

The change in the absorption spectra between oxyhemoglobin and deoxyhemoglobin enabled the total concentration of hemoglobin and the oxygen saturation in the rodent brain vasculature or tumor angiogenesis to be detected in multiwavelength PAM [37, 45–47]. Gold nanoparticles (AuNPs) are exemplar PA contrast agents that provide unique possibilities for both in vitro and in vivo molecular PA imaging. For example, AuNPs have been administered to blood vessels for blood flow velocity measurements in chicken breast tissue [48, 49] and for monitoring the intravascular fluid pathway of the rat brain [50]. The use of NIR-responsive PA dyes for functional PA calcium imaging in in vitro 3D cell cultures and in vivo animal models, including arsenazo III, chlorophosphonazo III, and genetically encoded calcium indicators, has also been documented [51–53]. For in vivo

or ex vivo functional imaging or to observe flow dynamics in a fluid system, working with AR-PAM can achieve deeper imaging up to few millimeters and spatial resolution of 45–200 μm, but OR-PAM can provide cellular level information such as intracellular calcium imaging in 3D cell culture systems.

### Structural imaging of 3D scaffolds/tissues

After implanting 3D engineered porous scaffolds into mice ears, neovascularization in the implanted scaffolds could be noninvasively monitored and quantified using both AR-PAM and OR-PAM for up to 6 weeks [54]. Polymer porous 3D scaffolds incorporating carbon nanotubes or 3D-printed alginate-polydopamine scaffolds can be used for structural examinations of the 3D scaffolds with PA imaging [55, 56]. In these studies, to visualize the network of capillaries (5–10 μm) and 3D engineered porous scaffolds, OR-PAM is used to achieve spatial resolution of 5 μm and axial resolution of 15 μm, but with a limited imaging depth (1 mm). OR-PAM provides well-resolved images allowing quantification of the characteristics of the 3D scaffolds such as pore size, porosity, or fiber formation, and AR-PAM provides a thicker image layer up to 2 mm.

### Cell tracking and tumor cells detection in 3D cell cultures/tissues

Melanin, a naturally produced pigment in melanoma cells, provides good optical and PA contrast in melanoma relative

to the surrounding tissue, and allowed for tracing the melanoma cells and monitoring the melanoma growth for 2 weeks [57]. This property means that melanoma cells are traceable for monitoring cell proliferation in engineered 3D porous scaffolds [58]. Making use of cellular endocytosis processes, AuNPs can be loaded into stem cells or macrophages as a PA contrast agent, which opens the possibility of the long-term tracking and monitoring of stem cells or macrophages in a 3D fibrin or gelatin scaffold through multimodal US and PA imaging for utilization in investigations of stem cell therapy [59–65]. Nanoparticles are generally more likely to accumulate in a tumor lesion due to the enhanced permeability and retention of the leaky tumor blood vessels [66], which has been demonstrated by the passive targeting and accumulation of AuNPs at a tumor site [67]. For tracking cells or delivering the contrast agent to specific regions in order to reduce off-target effects, strategies for conjugating the targeting ligands such as antibodies, peptides, and aptamers with contrast agents for active targeting have been developed. AuNPs with molecular targeting ability such as those conjugated with antibodies recognized to tumor protein biomarkers, and Arg-Gly-Asp (RGD) peptide are also commonly applied for tumor detection in vivo in PA imaging [68–73]. Exploring the crosstalk between stromal ECM and T cells is important for the corresponding immunotherapy strategies. T cells that have taken up AuNPs or can be loaded in an in vitro 3D hydrogel for tracking individual T cells when migrating to tumorspheres with OR-PAM [74, 75]. T cells labeled with NIR-797-isothiocyanate (an NIR PA and fluorescent dye) can be applied to imaging the dynamic change of T cells in lymph nodes in an in vivo mouse model by using AR-PAM [76].

One interesting application of using PA exogenous contrast agents is detecting the PA signals of matrix metalloproteinase-2 (MMP-2) in follicular thyroid cancer [77]. MMP-2 is abundant in several kinds of tumor cells and is known to be closely associated with tumor progression and metastasis [78]. MMP-2 can be targeted by a modified activatable cell-penetrating peptide that is labeled with two chromophores exhibiting different optical absorption wavelengths: BHQ-3 (675 nm) and Alexa Fluor 750 (750 nm) [79]. Both chromophores can be detected photoacoustically. Once MMP-2 is cleaved, only the dye with the BHQ3-labeled cell-penetrating part of the probe accumulates in the cells, and the location of the cleaved probe is observable after background subtraction. These synthesized contrast agents were used to noninvasively detect the location of follicular thyroid cancer in a mouse model by using AR-PAM [77] and may be used in 3D tumor culture model as well.

### Bottlenecks and future prospects

To expand the capabilities of multimodality imaging, PAM could be combined with US imaging in image-guided tumor therapies for the purpose of theranostics. The use of both the PAM and US modalities provides anatomical and functional information [32, 80–83]. Contrast agents in multimodality imaging systems can enhance the contrast in two or more modalities. For example, the position of the sentinel lymph node can be displayed using US imaging, with PA imaging used to display the accumulation of methylene blue [83]. Combined PA and US imaging with PA contrast agents can be further applied in image-guided photothermal therapy [52, 71, 72]. An US system could be used to monitor the targeting of AuNPs-encapsulated microbubbles, with PA imaging used to monitor the US-assisted delivery of AuNPs at the tumor lesion [66]. Moreover, phase-shifted droplets can be used as the contrast agent to enhance the contrast of combined US and PA imaging and also the therapeutic effects [28, 84, 85]. These previous studies have mainly relied on an optical droplet vaporization mechanism, and deep explorations of the underlying physics are now required to further optimize these techniques. The potential bioeffects should also be determined to ensure safety. A very recent phantom study employed the cancer drug doxorubicin as a PA contrast agent has shed more light on tumor theranostics [86]. Further phantom and in vitro 3D cell culture validations should be performed to improve these methods with consideration of the tissue complexity before moving to clinical applications.

Another aspect of PA imaging in a 3D cell microenvironment that needs further work is improving the imaging frame rate with the aim of achieving real-time functional applications, especially in thick 3D scaffolds. For example, acoustic-lens-based PA imaging [87, 88] and optical US mapping [89] open up new possibilities to increase the imaging speed, spatial resolution, and field of view. Finally, quantitative studies for standardizing preclinical applications are also important for translating the present results to the clinic.

### Conclusions

PA imaging has been investigated in preclinical studies over the past decade. This review has described the current state of PA imaging, focusing on the application of PA imaging techniques to a 3D cellular microenvironment. PA imaging provides a better penetration depth and can yield both structural and functional information of 3D biological samples from the single-cell level to the organoid level. Combining a multiwavelength laser with the use of contrast agents can produce multicontrast images. Hence, PA imaging has been developed as a powerful tool to dissect the mechanisms underlying spatiotemporal development in preclinical studies. However, it is difficult to compare the results obtained from different 3D cell

culture systems and PA imaging systems due to the wide range of the in-house systems that are available. Future works will focus on quantitative studies by using various types of PA imaging systems to achieve standardization of each biological characteristic in different 3D cell culture samples.

### Abbreviations

2D: Two-dimensional; 3D: Three-dimensional; AR-PAM: Acoustic-resolution microscopy; AuNPs: Gold nanoparticles; CM: confocal microscopy; ECM: Extracellular matrix; EM: electron microscopy; MMP-2: Matrix metalloproteinase-2; MPM: multi-photon microscopy; NIR: Near-infrared; OCT: optical coherence tomography.; OR-PAM: Optical-resolution microscopy; PA: Photoacoustic; RGD peptide: Arg-Gly-Asp peptidePAMPhotoacoustic microscopy; US: Ultrasound; YAP: Yes-associated protein

### References
1. Duval K, Grover H, Han LH, Mou Y, Pegoraro AF, Fredberg J, et al. Modeling physiological events in 2D vs. 3D cell culture. Physiology (Bethesda). 2017; 32:266–77.
2. Gillet JP, Calcagno AM, Varma S, Marino M, Green LJ, Vora MI, et al. Redefining the relevance of established cancer cell lines to the study of mechanisms of clinical anti-cancer drug resistance. Proc Natl Acad Sci U S A. 2011;108:18708–13.
3. Katt ME, Placone AL, Wong AD, Xu ZS, Searson PC. In vitro tumor models: advantages, disadvantages, variables, and selecting the right platform. Front Bioeng Biotechnol. 2016;4:12.
4. Liu Y, Chen YG. 2D- and 3D-based intestinal stem cell cultures for personalized medicine. Cells. 2018;7:225.
5. Yamada KM, Cukierman E. Modeling tissue morphogenesis and cancer in 3D. Cell. 2007;130:601–10.
6. Chen Q, Liu G, Liu S, Su H, Wang Y, Li J, et al. Remodeling the tumor microenvironment with emerging Nanotherapeutics. Trends Pharmacol Sci. 2018;39:59–74.
7. Di Modugno F, Colosi C, Trono P, Antonacci G, Ruocco G, Nistico P. 3D models in the new era of immune oncology: focus on T cells, CAF and ECM. J Exp Clin Cancer Res. 2019;38:117.
8. Song HH, Park KM, Gerecht S. Hydrogels to model 3D in vitro microenvironment of tumor vascularization. Adv Drug Deliv Rev. 2014;79–80:19–29.
9. Bougherara H, Mansuet-Lupo A, Alifano M, Ngo C, Damotte D, Le Frere-Belda MA, et al. Real-time imaging of resident T cells in human lung and ovarian carcinomas reveals how different tumor microenvironments control T lymphocyte migration. Front Immunol. 2015;6:500.
10. Hartmann N, Giese NA, Giese T, Poschke I, Offringa R, Werner J, et al. Prevailing role of contact guidance in intrastromal T-cell trapping in human pancreatic cancer. Clin Cancer Res. 2014;20:3422–33.
11. Salmon H, Franciszkiewicz K, Damotte D, Dieu-Nosjean MC, Validire P, Trautmann A, et al. Matrix architecture defines the preferential localization and migration of T cells into the stroma of human lung tumors. J Clin Invest. 2012;122:899–910.
12. Wolf K, Muller R, Borgmann S, Brocker EB, Friedl P. Amoeboid shape change and contact guidance: T-lymphocyte crawling through fibrillar collagen is independent of matrix remodeling by MMPs and other proteases. Blood. 2003;102:3262–9.
13. Wolf K, Te Lindert M, Krause M, Alexander S, Te Riet J, Willis AL, et al. Physical limits of cell migration: control by ECM space and nuclear deformation and tuning by proteolysis and traction force. J Cell Biol. 2013;201:1069–84.
14. Kuczek DE, Larsen AMH, Thorseth ML, Carretta M, Kalvisa A, Siersbaek MS, et al. Collagen density regulates the activity of tumor-infiltrating T cells. J Immunother Cancer. 2019;7:68.
15. Edsparr K, Basse PH, Goldfarb RH, Albertsson P. Matrix metalloproteinases in cytotoxic lymphocytes impact on tumour infiltration and immunomodulation. Cancer Microenviron. 2011;4:351–60.
16. Folkman J. Role of angiogenesis in tumor growth and metastasis. Semin Oncol. 2002;29(6 Suppl 16):15–8.
17. Oh S, Ryu H, Tahk D, Ko J, Chung Y, Lee HK, et al. "open-top" microfluidic device for in vitro three-dimensional capillary beds. Lab Chip. 2017;17:3405–14.
18. Paek J, Park SE, Lu Q, Park KT, Cho M, Oh JM, et al. Microphysiological engineering of self-assembled and Perfusable microvascular beds for the production of vascularized three-dimensional human microtissues. ACS Nano. 2019;13:7627–43.
19. Chen MB, Lamar JM, Li R, Hynes RO, Kamm RD. Elucidation of the roles of tumor integrin beta1 in the extravasation stage of the metastasis Cascade. Cancer Res. 2016;76:2513–24.
20. Zervantonakis IK, Hughes-Alford SK, Charest JL, Condeelis JS, Gertler FB, Kamm RD. Three-dimensional microfluidic model for tumor cell intravasation and endothelial barrier function. Proc Natl Acad Sci U S A. 2012;109:13515–20.
21. Amann A, Zwierzina M, Koeck S, Gamerith G, Pechriggl E, Huber JM, et al. Development of a 3D angiogenesis model to study tumour - endothelial cell interactions and the effects of anti-angiogenic drugs. Sci Rep. 2017;7:2963.
22. Park JS, Kim IK, Han S, Park I, Kim C, Bae J, et al. Normalization of tumor vessels by Tie2 activation and Ang2 inhibition enhances drug delivery and produces a favorable tumor microenvironment. Cancer Cell. 2016;30:953–67.
23. Rao SS, Bentil S, DeJesus J, Larison J, Hissong A, Dupaix R, et al. Inherent interfacial mechanical gradients in 3D hydrogels influence tumor cell behaviors. PLoS One. 2012;7:e35852.
24. Lee JY, Chang JK, Dominguez AA, Lee HP, Nam S, Chang J, et al. YAP-independent mechanotransduction drives breast cancer progression. Nat Commun. 2019;10:1848.
25. Su JL, Wang B, Wilson KE, Bayer CL, Chen YS, Kim S, et al. Advances in clinical and biomedical applications of Photoacoustic imaging. Expert Opin Med Diagn. 2010;4:497–510.
26. Wang LV, Hu S. Photoacoustic tomography: in vivo imaging from organelles to organs. Science. 2012;335:1458–62.
27. Beard P. Biomedical photoacoustic imaging. Interface Focus. 2011;1:602–31.
28. Fernandes DA, Kolios MC. Intrinsically absorbing photoacoustic and ultrasound contrast agents for cancer therapy and imaging. Nanotechnology. 2018;29:505103.
29. Weber J, Beard PC, Bohndiek SE. Contrast agents for molecular photoacoustic imaging. Nat Methods. 2016;13:639–50.
30. Yao J, Wang L, Yang JM, Maslov KI, Wong TT, Li L, et al. High-speed label-free functional photoacoustic microscopy of mouse brain in action. Nat Methods. 2015;12:407–10.
31. Hai P, Imai T, Xu S, Zhang R, Aft RL, Zou J, et al. High-throughput, label-free, single-cell photoacoustic microscopy of intratumoral metabolic heterogeneity. Nat Biomed Eng. 2019;3:381–91.
32. Mallidi S, Luke GP, Emelianov S. Photoacoustic imaging in cancer detection, diagnosis, and treatment guidance. Trends Biotechnol. 2011;29:213–21.
33. Jathoul AP, Laufer J, Ogunlade O, Treeby B, Cox B, Zhang E, et al. Deep in vivo photoacoustic imaging of mammalian tissues using a tyrosinase-based genetic reporter. Nat Photonics. 2015;9:239.
34. Zhou Y, Yao J, Wang LV. Tutorial on photoacoustic tomography. J Biomed Opt. 2016;21:61007.

35. Wang LV. Tutorial on Photoacoustic microscopy and computed tomography. IEEE J Sel Top Quantum Electron. 2008;14:171–9.
36. Hatamimoslehabadi M, Bellinger S, La J, Ahmad E, Frenette M, Yelleswarapu C, et al. Correlation of Photophysical properties with the Photoacoustic emission for a selection of established Chromophores. J Phys Chem C. 2017; 121:24168–78.
37. Kim C, Erpelding TN, Jankovic L, Pashley MD, Wang LV. Deeply penetrating in vivo photoacoustic imaging using a clinical ultrasound array system. Biomed Opt Express. 2010;1:278–84.
38. Song KH, Wang LV. Deep reflection-mode photoacoustic imaging of biological tissue. J Biomed Opt. 2007;12:060503.
39. Zhang HF, Maslov K, Stoica G, Wang LV. Functional photoacoustic microscopy for high-resolution and noninvasive in vivo imaging. Nat Biotechnol. 2006;24:848–51.
40. Maslov K, Zhang HF, Hu S, Wang LV. Optical-resolution photoacoustic microscopy for in vivo imaging of single capillaries. Opt Lett. 2008;33:929–31.
41. Zhang C, Maslov K, Yao J, Wang LV. In vivo photoacoustic microscopy with 7.6-μm axial resolution using a commercial 125-MHz ultrasonic transducer. J Biomed Opt. 2012;17:116016.
42. Zhang C, Maslov K, Wang LV. Subwavelength-resolution label-free photoacoustic microscopy of optical absorption in vivo. Opt Lett. 2010;35:3195–7.
43. Yao J, Wang L, Li C, Zhang C, Wang LV. Photoimprint photoacoustic microscopy for three-dimensional label-free subdiffraction imaging. Phys Rev Lett. 2014;112:014302.
44. Yao J, Wang LV. Sensitivity of photoacoustic microscopy. Photoacoustics. 2014;2:87–101.
45. Gamelin J, Maurudis A, Aguirre A, Huang F, Guo P, Wang LV, et al. A real-time photoacoustic tomography system for small animals. Opt Express. 2009;17:10489–98.
46. Chen SL, Burnett J, Sun D, Wei X, Xie Z, Wang X. Photoacoustic microscopy: a potential new tool for evaluation of angiogenesis inhibitor. Biomed Opt Express. 2013;4:2657–66.
47. Ku G, Wang X, Xie X, Stoica G, Wang LV. Imaging of tumor angiogenesis in rat brains in vivo by photoacoustic tomography. Appl Opt. 2005;44:770–5.
48. Liao CK, Huang SW, Wei CW, Li PC. Nanorod-based flow estimation using a high-frame-rate photoacoustic imaging system. J Biomed Opt. 2007;12:064006.
49. Wei CW, Huang SW, Wang CR, Li PC. Photoacoustic flow measurements based on wash-in analysis of gold nanorods. IEEE Trans Ultrason Ferroelectr Freq Control. 2007;54:1131–41.
50. Wang Y, Xie X, Wang X, Ku G, Gill KL, O'Neal DP, et al. Photoacoustic tomography of a Nanoshell contrast agent in the in vivo rat brain. Nano Lett. 2004;4:1689–92.
51. Dean-Ben XL, Gottschalk S, Sela G, Shoham S, Razansky D. Functional optoacoustic neuro-tomography of calcium fluxes in adult zebrafish brain in vivo. Opt Lett. 2017;42:959–62.
52. Liu W-W, Chen S-H, Li P-C. Functional calcium imaging using optical-resolution photoacoustic microscopy in a 3D tumor cell culture. Proc SPIE. 2019. https://doi.org/10.1117/12.2510936.
53. Dana N, Fowler RA, Allen A, Zoldan J, Suggs L, Emelianov S. In vitro photoacoustic sensing of calcium dynamics with arsenazo III. Laser Phys Lett. 2016;13:075603.
54. Cai X, Zhang Y, Li L, Choi SW, MacEwan MR, Yao J, et al. Investigation of neovascularization in three-dimensional porous scaffolds in vivo by a combination of multiscale photoacoustic microscopy and optical coherence tomography. Tissue Eng Part C Methods. 2013;19:196–204.
55. Cai X, Paratala BS, Hu S, Sitharaman B, Wang LV. Multiscale photoacoustic microscopy of single-walled carbon nanotube-incorporated tissue engineering scaffolds. Tissue Eng Part C Methods. 2012;18:310–7.
56. Luo Y, Wei X, Wan Y, Lin X, Wang Z, Huang P. 3D printing of hydrogel scaffolds for future application in photothermal therapy of breast cancer and tissue repair. Acta Biomater. 2019;92:37–47.
57. Staley J, Grogan P, Samadi AK, Cui H, Cohen MS, Yang X. Growth of melanoma brain tumors monitored by photoacoustic microscopy. J Biomed Opt. 2010;15:040510.
58. Zhang Y, Cai X, Choi SW, Kim C, Wang LV, Xia Y. Chronic label-free volumetric photoacoustic microscopy of melanoma cells in three-dimensional porous scaffolds. Biomaterials. 2010;31:8651–8.
59. Chung E, Nam SY, Ricles LM, Emelianov SY, Suggs LJ. Evaluation of gold nanotracers to track adipose-derived stem cells in a PEGylated fibrin gel for dermal tissue engineering applications. Int J Nanomedicine. 2013;8:325–36.
60. Li W, Chen X. Gold nanoparticles for photoacoustic imaging. Nanomedicine (Lond). 2015;10:299–320.
61. Jokerst JV, Thangaraj M, Kempen PJ, Sinclair R, Gambhir SS. Photoacoustic imaging of mesenchymal stem cells in living mice via silica-coated gold nanorods. ACS Nano. 2012;6:5920–30.
62. Kubelick KP, Snider EJ, Ethier CR, Emelianov S. Development of a stem cell tracking platform for ophthalmic applications using ultrasound and photoacoustic imaging. Theranostics. 2019;9:3812–24.
63. Ricles LM, Hsieh PL, Dana N, Rybalko V, Kraynak C, Farrar RP, et al. Therapeutic assessment of mesenchymal stem cells delivered within a PEGylated fibrin gel following an ischemic injury. Biomaterials. 2016;102:9–19.
64. Nam SY, Ricles LM, Suggs LJ, Emelianov SY. In vivo ultrasound and photoacoustic monitoring of mesenchymal stem cells labeled with gold nanotracers. PLoS One. 2012;7:e37267.
65. Dhada KS, Hernandez DS, Suggs LJ. In vivo Photoacoustic tracking of Mesenchymal stem cell viability. ACS Nano. 2019;13:7791–9.
66. Matsumura Y, Maeda H. A new concept for macromolecular therapeutics in cancer chemotherapy: mechanism of tumoritropic accumulation of proteins and the antitumor agent smancs. Cancer Res. 1986;46:6387–92.
67. Srivatsan A, Jenkins SV, Jeon M, Wu Z, Kim C, Chen J, et al. Gold nanocage-photosensitizer conjugates for dual-modal image-guided enhanced photodynamic therapy. Theranostics. 2014;4:163–74.
68. Nie L, Wang S, Wang X, Rong P, Ma Y, Liu G, et al. In vivo volumetric photoacoustic molecular angiography and therapeutic monitoring with targeted plasmonic nanostars. Small. 2014;10:1585–93.
69. Li PC, Wang CR, Shieh DB, Wei CW, Liao CK, Poe C, et al. In vivo photoacoustic molecular imaging with simultaneous multiple selective targeting using antibody-conjugated gold nanorods. Opt Express. 2008;16: 18605–15.
70. Cheng K, Kothapalli SR, Liu H, Koh AL, Jokerst JV, Jiang H, et al. Construction and validation of nano gold tripods for molecular imaging of living subjects. J Am Chem Soc. 2014;136:3560–71.
71. Wang YH, Chen SP, Liao AH, Yang YC, Lee CR, Wu CH, et al. Synergistic delivery of gold nanorods using multifunctional microbubbles for enhanced plasmonic photothermal therapy. Sci Rep. 2014;4:5685.
72. Wang YH, Liao AH, Chen JH, Wang CR, Li PC. Photoacoustic/ultrasound dual-modality contrast agent and its application to thermotherapy. J Biomed Opt. 2012;17:045001.
73. Agarwal A, Huang SW, O'Donnell M, Day KC, Day M, Kotov N, et al. Targeted gold nanorod contrast agent for prostate cancer detection by photoacoustic imaging. J Appl Phys. 2007;102:064701.
74. Lee PY, Liu WW, Chen SC, Li PC. Dual-wavelength optical-resolution photoacoustic microscopy for cells with gold nanoparticle bioconjugates in three-dimensional cultures. Proc SPIE. 2016. https://doi.org/10.1117/12.2214037.
75. Huang RX, Fu Y, Liu W, Ma YT, Hsieh B-Y, Chen SC, et al. Dual-wavelength OR-PAM with compressed sensing for cell tracking in a 3D cell culture system. Proc SPIE. 2018. https://doi.org/10.1117/12.2289975.
76. Zheng S, Li H, Lai K, Chen M, Fu G, Liu WH, et al. Noninvasive photoacoustic and fluorescent tracking of optical dye labeled T cellular activities of diseased sites at new depth. J Biophotonics. 2018;11:e201800073.
77. Levi J, Kothapalli SR, Bohndiek S, Yoon JK, Dragulescu-Andrasi A, Nielsen C, et al. Molecular photoacoustic imaging of follicular thyroid carcinoma. Clin Cancer Res. 2013;19:1494–502.
78. Coussens LM, Fingleton B, Matrisian LM. Matrix metalloproteinase inhibitors and cancer: trials and tribulations. Science. 2002;295:2387–92.
79. Levi J, Kothapalli SR, Ma TJ, Hartman K, Khuri-Yakub BT, Gambhir SS. Design, synthesis, and imaging of an activatable photoacoustic probe. J Am Chem Soc. 2010;132:11264–9.
80. Kolkman RG, Brands PJ, Steenbergen W, van Leeuwen TG. Real-time in vivo photoacoustic and ultrasound imaging. J Biomed Opt. 2008;13:050510.
81. Wilson K, Homan K, Emelianov S. Biomedical photoacoustics beyond thermal expansion using triggered nanodroplet vaporization for contrast-enhanced imaging. Nat Commun. 2012;3:618.
82. Harrison T, Ranasinghesagara JC, Lu H, Mathewson K, Walsh A, Zemp RJ. Combined photoacoustic and ultrasound biomicroscopy. Opt Express. 2009; 17:22041–6.
83. Erpelding TN, Kim C, Pramanik M, Jankovic L, Maslov K, Guo Z, et al. Sentinel lymph nodes in the rat: noninvasive photoacoustic and US imaging with a clinical US system. Radiology. 2010;256:102–10.
84. Chen Q, Yu J, Kim K. Review: optically-triggered phase-transition droplets for photoacoustic imaging. Biomed Eng Lett. 2018;8:223–9.

85. Liu WW, Huang SH, Li PC. Synchronized optical and acoustic droplet vaporization for effective Sonoporation. Pharmaceutics. 2019;11:279.

86. Kimm MA, Gross C, Dean-Ben XL, Ron A, Rummeny EJ, Lin HA, et al. Optoacoustic properties of doxorubicin - a pilot study. PLoS One. 2019;14:e0217576.

87. He Y, Tang Z, Chen Z, Wan W, Li J. A novel photoacoustic tomography based on a time-resolved technique and an acoustic lens imaging system. Phys Med Biol. 2006;51:2671–80.

88. Dogra VS, Chinni BK, Valluru KS, Moalem J, Giampoli EJ, Evans K, et al. Preliminary results of ex vivo multispectral photoacoustic imaging in the management of thyroid cancer. AJR Am J Roentgenol. 2014;202:W552–8.

89. Zhang E, Laufer J, Beard P. Backward-mode multiwavelength photoacoustic scanner using a planar Fabry-Perot polymer film ultrasound sensor for high-resolution three-dimensional imaging of biological tissues. Appl Opt. 2008;47:561–77.

## Publisher's Note